Chapter 9

# Compact Planar Antennas for Beam Steering and RFID Tags

Mohammad Alibakhshi-Kenari,
Mohammad Naser-Moghadasi,
Ramazan Ali Sadeghzadeh, Bal Singh Virdee and
Ernesto Limiti

Additional information is available at the end of the chapter

http://dx.doi.org/10.5772/65918

**Abstract**

The chapter presents innovative planar antennas for beam steering and radio frequency identification (RFID) applications. Beam steering has become vital in commercial wireless communications, including mobile satellite communications where high data rate communication is required. The chapter describes a low-cost beam-steering antenna based on a leaky-wave antenna structure that is capable of steering the main radiation beam of the antenna over a large range from −30° to +15°. Interest in RFID systems operating in the ultrahigh frequency (UHF) is rapidly growing as it offers benefits of long read range and low cost, which make it an excellent system for use in distribution and logistics systems. This chapter presents a technique of overcoming the limitations of conventional HF coils in RFID tags where the total length of the spiral antenna is restricted inside the available area of the tag.

**Keywords:** leaky-wave antenna (LWA), broadside radiation, beam steering, RFID tag, Hilbert curve, HF/UHF dual-band antenna

## 1. Introduction

Sophisticated modern wireless systems have begun employing beam-scanning antennas to improve their coverage and hence increase system capacity. Antennas whose radiation beam can be steered by electronic means are therefore becoming highly desirable. Beam steering can be realized in antenna arrays by modifying the phase of the transmitted signal. The phase of the signal can be altered electronically with phase shifters.

Alternatively, this can be achieved using a leaky-wave antenna (LWA) in which the direction of the radiation beam is a function of the operating frequency [1–3]. In part 2, the design and experimental results are presented of a printed LWA. Features of the LWA include a simple structure, small size, low profile, large bandwidth (BW), high gain, and large beam steering from -30° to +15°. In part 3, an innovative dual-band card-type tag is presented that is based on a single-loop radiator. The card-tag design is implemented using Hilbert-curve for radio frequency identification (RFID)-positioning applications. The RFID tag radiator design is realized by combining the Hilbert curve and the square-loop radiator, where the Hilbert curve is designed to operate at HF band, and the square loop at ultrahigh-frequency (UHF) band.

## 2. Printed leaky-wave antenna design

The LWA, shown in **Figure 1**, can be considered a rectangular patch antenna with a rectangular dielectric slot. The bottom side of the antenna substrate is a ground plane. Within the slot are six radiating arms comprising E-shaped structures which are organized in three columns and two rows. The structure is excited through a subminiature version A (SMA) connector on one side, and the structure is terminated with a 50-Ω load on the opposite side. The bandwidth and radiation characteristics of the antenna can be controlled by simply modifying the number of E-shaped arms, their dimensions, and also the separation between them. The LWA antenna was analyzed by three full-wave EM simulators, that is, Agilent ADS, HFSS™, and CST-MWS. LWA prototype design presented was constructed on Rogers RT/Duroid5880 substrate with a thickness of 1.6 mm, a dielectric constant of 2.2, and tan δ of $9 \times 10^{-4}$. The optimized antenna design was fabricated and tested to validate its performance. The length, width, and height of the antenna are 19.2 ($59 \times 10^{-3}\lambda_o$), 15.2 ($47 \times 10^{-3}\lambda_o$), and 1.6 mm ($4 \times 10^{-3}\lambda_o$), respectively, where $\lambda_o$ is free-space wavelengths at 930 MHz.

**Figure 2** shows that the proposed LWA covers an impedance bandwidth (for $S_{11} < -10$ dB) of 2.81 GHz (0.90–3.71 GHz) with ADS; 2.95 GHz (0.93–3.88 GHz) with CST MWS; and 3.2 GHz (0.77–3.97 GHz) with HFSS™, which correspond to fractional bandwidth of 121.9, 122.6, and 135.0%, respectively. The measured impedance bandwidth is 2.72 GHz (0.93–3.65 GHz), which correspond to fractional bandwidth of 118.7%. There is generally good agreement between the simulated and measured results.

Besides the broadband bandwidth property of the antenna, another feature of this antenna is its ability to provide continuous scanning of its main beam over a large range from -30° to +15° with high gain across its entire operating range as shown in **Figure 3** and **Figure 4**. These results show that the antenna radiates at different angles at 1.2 and 1.88 GHz, and 2.65, and 3.4 GHz. As the frequency is increased, the scanned angle changes almost in a linear fashion, as shown in **Figure 5**. The measured antenna gain and radiation efficiency at various frequencies are given in **Table 1**. The gain and efficiency are larger than 6 dBi and 62% across the antenna's operating band.

http://dx.doi.org/10.5772/65918

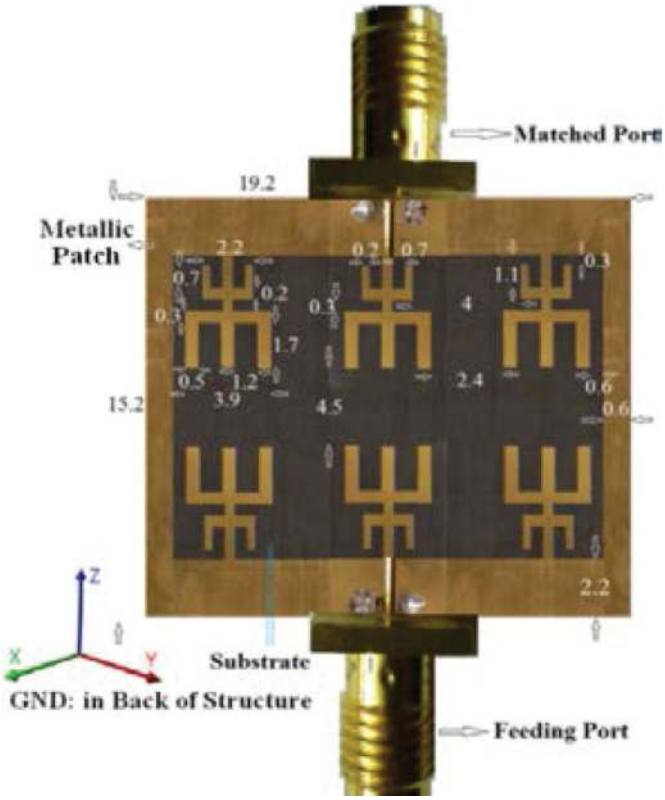


**Figure 1.** Fabricated prototype of the leaky-wave antenna (units in millimeters).

The maximum gain occurs at 2.65 GHz, that is, broadside radiation (**Figure 5**), and it remains between 8 and 6 dBi across the band, as shown in **Figure 6**. In addition to the scanning angle and gain curves versus frequency, the antenna gain curve as a function of scanning angle is given in **Figure 7**.

To summarize, the novel printed leaky-wave antenna structure presented above is capable of steering the main beam from -30° to +15°. The design of the antenna is based on several E-shaped-radiating arms implementing within the slot. The LWA is highly compact with dimensions of 19.2 × 15.2 × 1.6 $mm^3$, and has a large fractional bandwidth of 118.7% (0.93–3.65 GHz) with peak radiation gain and efficiency of 8 dBi and 90%, respectively, at 2.65 GHz. The proposed LWA can be flush-mounted on vehicles, laptops, cellular base-stations, and mobile phones. In addition, it can be easily integrated on different substrates for use in other circuits and devices. The broadside-radiating antenna is suitable for wireless communications systems.

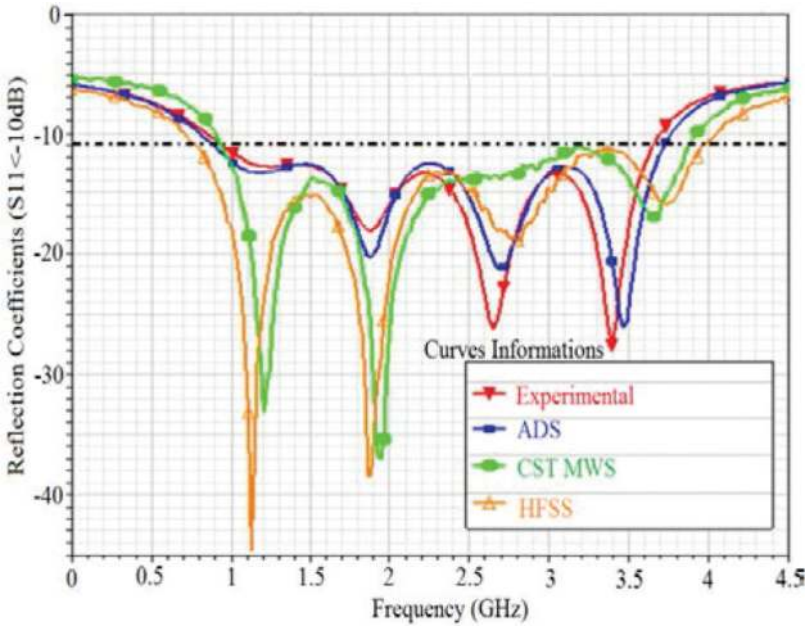


**Figure 2.** Simulated and measured reflection coefficients of the proposed LWA.

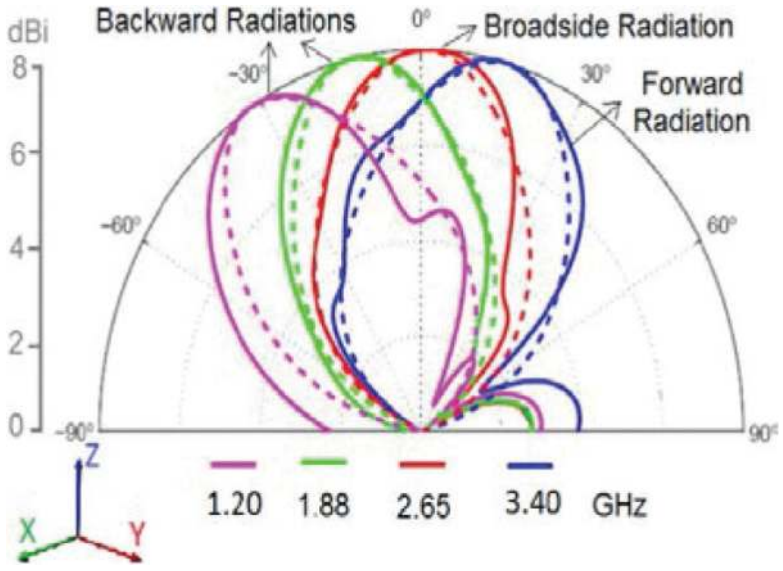


**Figure 3.** 2-D radiation patterns in dB scale at spot frequencies. Solid lines: measured results and dashed lines: simulated results.

http://dx.doi.org/10.5772/65918

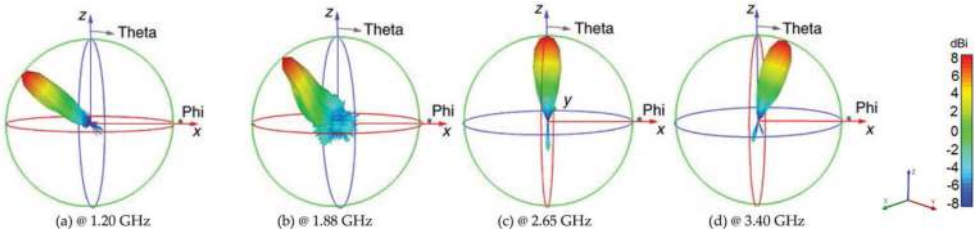


**Figure 4.** 3-D radiation patterns (decibel scale) at (a) 1.2 GHz, (b) 1.88 GHz, (c) 2.65, and (d) 3.40 GHz.

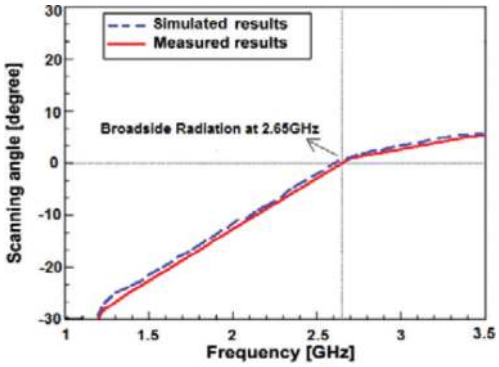


**Figure 5.** Scanning angle versus frequency. Broadside direction is 0°.

| Frequency (GHz) | 0.93 | 1.20 | 1.88 | 2.65 | 3.40 | 3.65 |
|---|---|---|---|---|---|---|
| Gain (dBi) | 6 | 7 | 7.7 | 8 | 7.8 | 7.2 |
| Efficiency (%) | 62 | 74 | 81 | 90 | 85 | 79 |

**Table 1.** Measured antenna radiation characteristics.

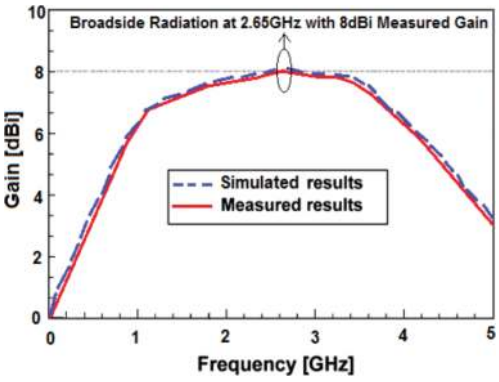


**Figure 6.** Gain as a function of frequency.

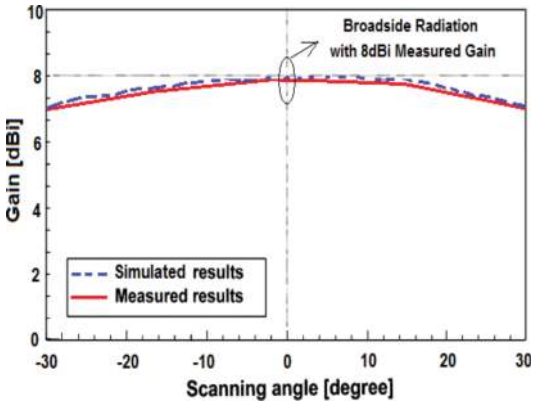


**Figure 7.** Gain curves versus scanning angle.

## 3. Dual-band RFID tag antenna

Based on the card-type dual-band tags [4–27], and the series Hilbert-curve tag, an alternative card-type dual-band RFID tag is proposed in this chapter. The proposed tag merges with the series Hilbert curve for HF coil antenna and square-loop patch for UHF antenna to form a single radiator that is compact and exhibits dual-band performance. The antenna's axial-ratio (AR) spectrum is shown to confirm its circular polarization characteristics.

The loop-tag antenna structure is based on the third-order Hilbert-fractal curve, and the antenna is impedance matched with a stub network, as shown in **Figure 8**. **Table 2** lists the parameters describing the antenna structure shown in **Figure 9**. The antenna was fabricated

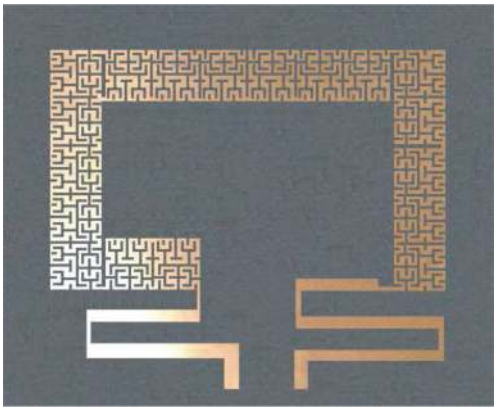

**Figure 8.** Fabricated Hilbert-curve loop RFID tag.

http://dx.doi.org/10.5772/65918

| $L_1$ | $L_2$ | $L_3$ | $L_4$ | $L_5$ | $L_6$ | $W_1$ | $W_2$ | $W_3$ | $W_4$ | $W_5$ | $W_6$ | $W_7$ | $W_8$ | $W_9$ | $W_{10}$ |
|---|---|---|---|---|---|---|---|---|---|---|---|---|---|---|---|
| 8 | 27.4 | 4 | 1.8 | 4.2 | 1.2 | 2.5 | 0.9 | 18.6 | 0.65 | 16.5 | 0.65 | 56 | 18 | 24 | 24.1 |

**Table 2.** Dimensions of Hilbert-curve loop RFID tag (units in millimeters).

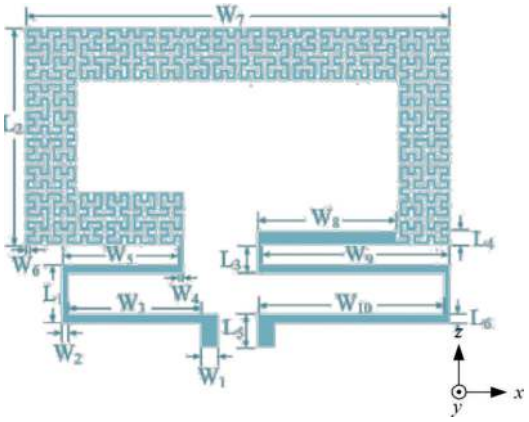


**Figure 9.** Parameters defining the RFID tag.

on Rogers/RT Duroid5880 dielectric substrate with a thickness ($h$) of 0.8 mm and a dielectric constant ($\varepsilon_r$) of 2.2.

The RFID tag, which is shown in **Figure 8**, operates over dual-band, in particular, the HF and UHF bands. Conventional RFID tags essentially comprise two distinct antennas [4–27], whereas the proposed dual-band structure employs one radiator that functions in the high frequency and ultrahigh-frequency bands.

### 3.1. High-frequency antenna

The series Hilbert-curve structure is used here as a HF coil antenna to implement the 25-MHz band RFID tag. When the plane of the coil is oriented perpendicular to the received magnetic field, it induces a voltage in the winding of the Hilbert-fractal curve. By increasing the area of the Hilbert curve, it will capture greater magnetic flux from the received signal; as a consequence greater voltage is induced in the coil. Hence, the space-filling fractal curve is recommended to occupy the RFID tag area as much as possible.

The total inductance and the resistive loss in the HF coil antenna determine its quality factor ($Q_{HF}$), which indicates energy loss relative to the amount of energy stored in the coil. The magnitude of $Q_{HF}$ increases with a decrease in loss. The quality factor of the antenna can be easily measured as it is related to the antenna's center frequency ($f_0$) and 3-dB bandwidth (BW) by the relationship $Q_{HF} = f_0/\text{BW}$. Also, the resonant frequency of the HF coil is a function of the coil's inductance and the capacitance, and is represented by the relationship $f_0 = 1/2\sqrt{\text{LC}}$.

### 3.2. Ultra high-frequency antenna

The length of the loop resonator is the fundamental design parameter of the proposed Hilbert-curve UHF antenna as it determines the self-resonant frequency of the antenna. In the design, the length of the loop resonator is folded within a defined area. By stimulating the loop with an electric field, a standing wave is excited in the loop. The resulting electric current flowing through the conductive loop causes the tag to radiate. The current distributions over the tag reveal the characteristics of the HF/UHF dual-band antenna. To optimize power transfer to or from the tag, it is necessary to properly match it to the microchip. This can be accomplished by using a microstrip network instead of using discrete lumped inductances and capacitances because at UHF the lumped components perform poorly due to generation of parasitic reactance.

### 3.3. Simulation and measured results

The simulated and measured return-loss responses of the proposed RFID tag are shown in **Figure 10**. Commercial software (HFSS) by Ansys was used to simulate the return loss of the antenna [28]. It is evident that there is excellent agreement between the simulation and measurement results. Measurements confirm that the RFID tag can operate over the frequency ranges of 12.5–37.5 MHz and 0.4–1.4 GHz for return-loss performance better than -10 dB. The four resonant modes have a center frequency of $f_c$ = 25 MHz, $f_c$= 785 MHz (760–815 MHz), 835 GHz (822–905 MHz), and 925 MHz (918–1000 MHz). These results show that the proposed RFID tag is suitable for dual-band applications in the HF and UHF bands. In addition, the band centered at 25 MHz shown in **Figure 10** is applicable for near-field communication (NFC).

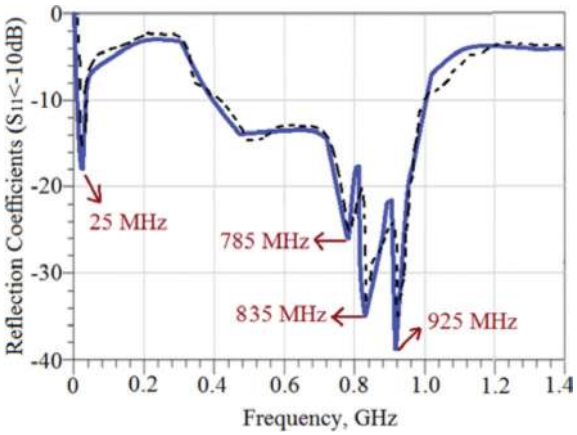


**Figure 10.** Simulated (solid-line) and measured (dashed-line) reflection-coefficient response.

The results of the impedance analysis, shown in **Figure 11**, reveal that the real-part of the impedance has a maximum magnitude of 49, 50, and 48Ω at 785, 835,and 925 MHz, respectively. The imaginary part of the impedance presents an inductive of magnitude 9, 8, and 11Ω

http://dx.doi.org/10.5772/65918

at 785, 835, and 925 MHz, respectively. Inductive impedance was used to impedance match the capacitive RFID microchip. At 25 MHz, the real part of the impedance is 2Ω, and the imaginary part is 40Ω, as shown in **Figure 11**. For the tag antenna impedance $Z_{A(HF)}$ = RA + jXA, the qualityfactor ($Q_A$) is expressed by

$$Q_A = X_A / R_A \tag{1}$$

The quality factor ($Q_A$) indicates that when the antenna is close to its resonance frequency, its impedance is almost real.

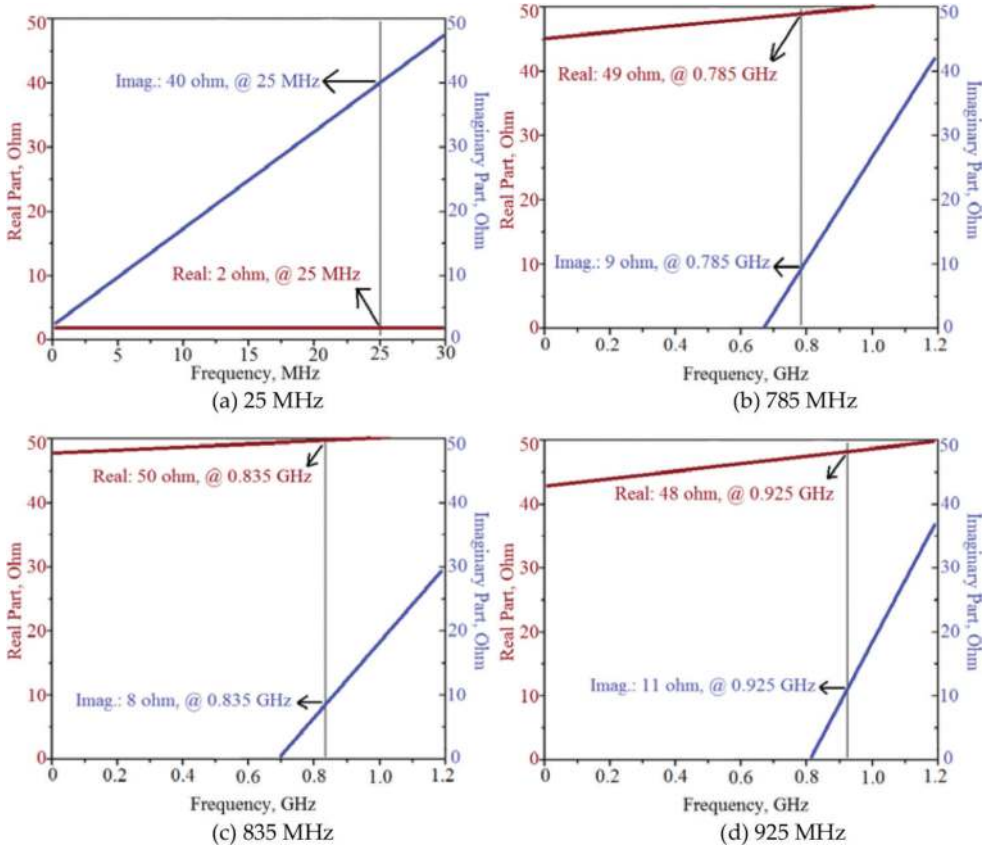


**Figure 11.** Measured results of impedance spectrum at (a) 25, (b) 785, (c) 835, and (d) 925 MHz.

The antenna is matched to the RFID microchip with an *LC* circuit to achieve a $Q_A$ of 25.1 at 25 MHz. The quality factors ($Q_A$) from **Figure 11** are as follows: 0.15, 0.17, and 0.165 at 785, 835, and 925 MHz, respectively. Distribution of the current density over the planar antenna, shown in **Figure 12**, gives insight of how the proposed dual-band antenna affects the current at the various frequencies. In **Figure 12**, the total length of the series Hilbert-curve loop

is 1/20 $\lambda_g$, and the mean circumstance of the loop in **Figure 12** is $\lambda_g$. The antenna belongs to the small antenna category as the total length of series Hilbert curve is less than 1/10 $\lambda_g$.

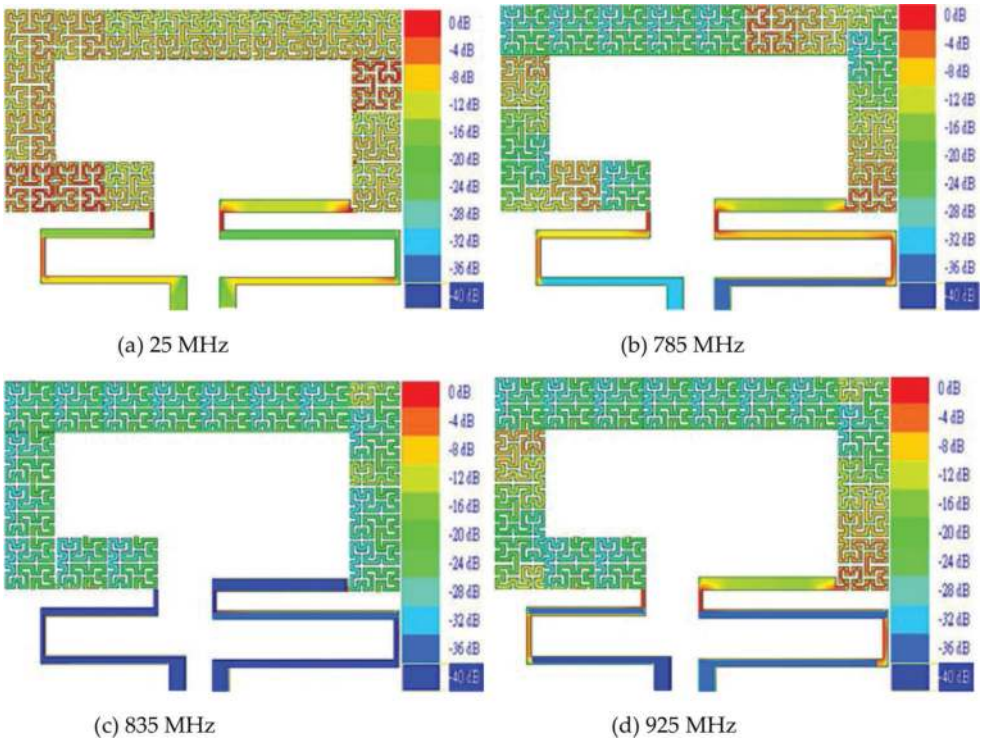


**Figure 12.** Current distributions at (a) 25, (b) 785, (c) 835, and (d) 925 MHz.

When the antenna was tested, it was aligned in the *zx*-plane as defined in **Figure 9** with the feed-line along the *x*-axis. Automatic measurement system in an anechoic chamber was used to measure the radiation pattern of the antenna. Radiation patterns of the RFID tag antenna were measured in the *xz*- and *yz*-planes. The radiation patterns at 25, 785, 835, and 925 MHz in the HF/UHF bands are depicted in **Figure 13**.

Simulated and measured radiation patterns of the RFID tag antenna in the *xz*- and *yz*-planes at 25, 785, 835, and 925 MHz over the HF/UHF bands are shown in **Figure 13**. Good agreement is obtained between the simulation and measured results. Measurements show that the radiation in the *xz*-plane is quasi omnidirectional at 25, 785, and 835 MHz; however, the radiation is bidirectional at 925 GHz. In the *yz*-plane, the radiation is omnidirectional at 25, 785, and 925 MHz, and is clearly bidirectional at 835 MHz. **Figure 14** shows that the directivity of the RFID tag antenna is 1.75 dBi at 25 MHz in the HF band, and 2.65, 2.82, and 2.75 dBi at 785, 835, and 925 MHz, respectively, in the UHF band.

http://dx.doi.org/10.5772/65918

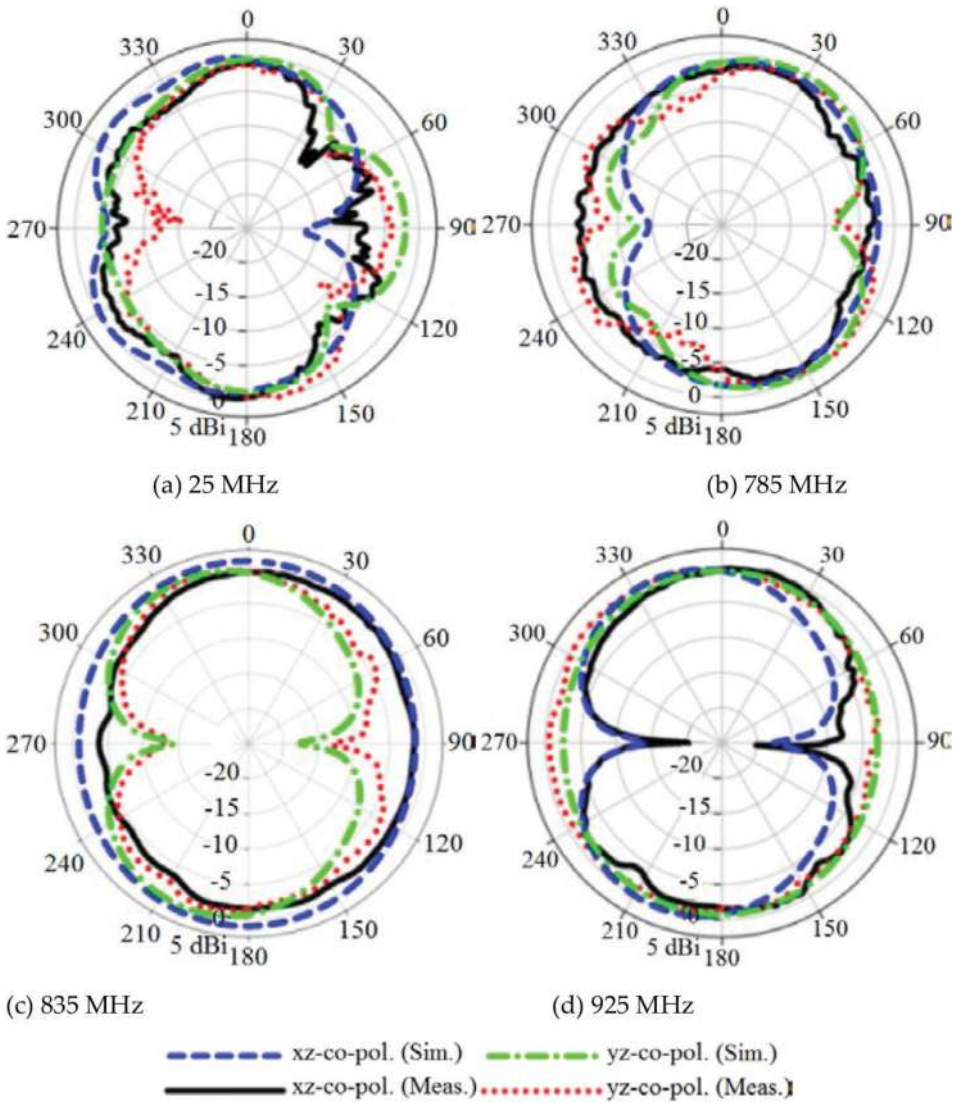


**Figure 13.** Radiation patterns of the RFID tag at: (a) 25, (b) 785, (c) 835, and (d) 925 MHz.

Circular polarization wave is generated by exciting two orthogonal modes in the RFID tag. This is achieved with the orthogonal arrangement of the Hilbert-curve tag. The axial-ratio spectrum of the polarization related to various angles ($\phi$ and $\theta$) is presented in **Figure 15**. The minimum axial ratio is observed at 785, 835, and 925 MHz at $\phi = 0^{\circ}$, $\theta = 95^{\circ}$ with corresponding -3-dB AR

bandwidth of 480 (560–1040 MHz), 605 (515–1120 MHz), and 455 MHz (620–1075 MHz). The minimum AR is observed at 25 MHz at $\phi = 0^{\circ}$, $\theta = 92^{\circ}$ with corresponding -3-dB AR bandwidth of 14 MHz (18–32 MHz). Thus, the proposed antenna can be applied to diversity operation.

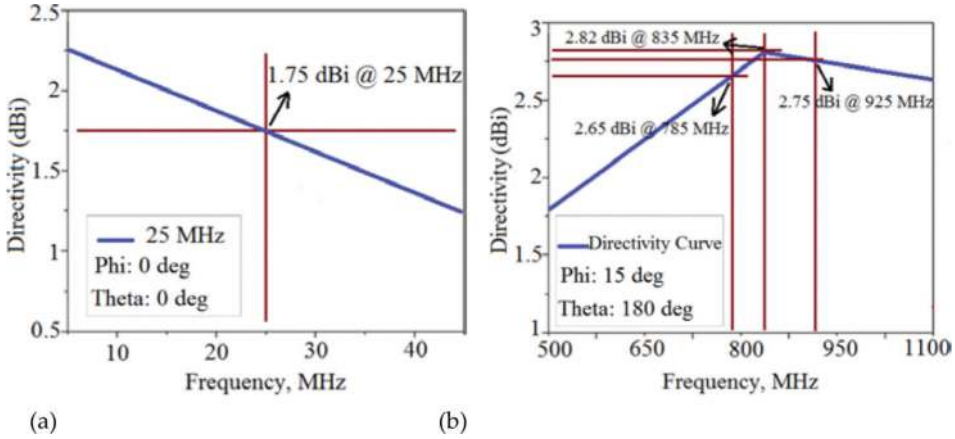


**Figure 14.** Directivity at (a) 25 MHz in the HF band, and (b) 785, 835, and 925 MHz in the UHF bands.

### 3.4. UHF-matching circuit

The maximum activation distance of the tag for the given frequency is given by [29, 30]

$$d_{\max} = \frac{c}{4\pi f}\sqrt{\frac{\mathrm{EIRP}_r}{P_{\mathrm{chip}}}\tau G} \tag{2}$$

where $\mathrm{EIRP}_r$ is the effective transmitted power of the reader, $P_{\mathrm{chip}}$ is the sensitivity of the tag microchip, $G$is the maximum tag antenna gain, and the power transmission factor $\tau$ is given by

$$\tau = \frac{4R_{\mathrm{tag}}R_A}{\left|X_{\mathrm{chip}} + X_A\right|^2} \le 1 \tag{3}$$

where the tag antenna impedance is $Z_{\mathrm{A(UHF)}} = R_{\mathrm{A}} + j\,X_{\mathrm{A}}$ and microchip impedance $Z_{\mathrm{chip}} = R_{\mathrm{chip}} + j\,X_{\mathrm{chip}}$.

The microchip NSC MM9647 can be applied to the tag in UHF band. Its impedance is $Z_{\mathrm{chip}}$ = 80 – *j* 120 Ω [31]. The effective isotropic radiated power ($EIRP_t$) of the reader is 1.2 W, the sensitivity $P_{\mathrm{chip}}$ of tag microchip is -10 dBm, the maximum tag antenna gain $G$ = 3.35 dBi, and the activation distance $d$with is $d_{\max}$ = 5 m. Therefore, from Eq. (2), the power transmission factor $\tau$ is 0.95. The tag antenna impedance from **Figure 11** is $Z_{A(\mathrm{UHF})}$ = 49 + *j*9 Ω at 785 MHz, $Z_{\mathrm{A(UHF)}}$ = 50+ *j* 8Ω at 835 MHz, and $Z_{\mathrm{A(UHF)}}$ = 48+ *j* 11Ω at 925 MHz; hence from Eq. (3), the RFID's microchip impedance of $Z_{\mathrm{chip}}$ = 80 – *j*Ω enables conjugate matching to be obtained.

http://dx.doi.org/10.5772/65918

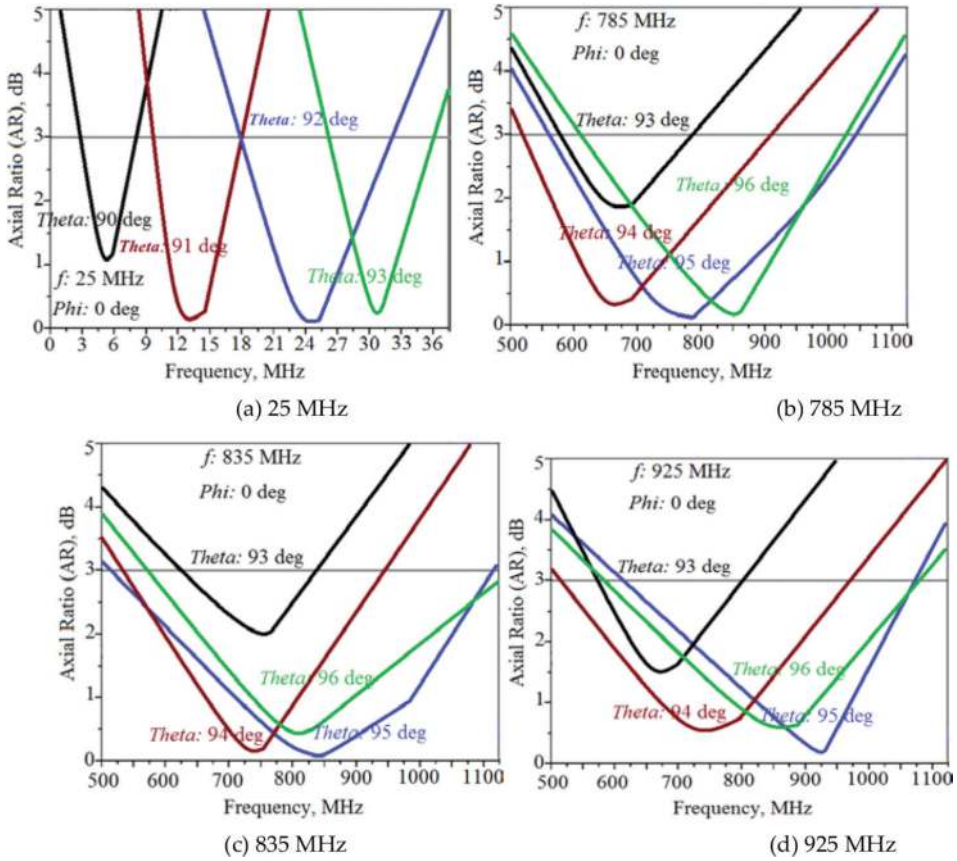


**Figure 15.** Axial-ratio spectrum centered at: (a) 25, (b) 785, (c) 835, and (d) 925 MHz.

### 3.5. HF-matching circuit

Another example of designing a matching network is presented using Tag-it$_{TM}$ HF-I standard transponder microchip which has capacitance $C_{chip}$ = 2.85 pF at 25 MHz [32]. The tag antenna's impedance from **Figure 11 (a)** is$Z_{A(HF)} = 2 + j\,40\Omega$, where $L_A = 0.45$ μH and $R_A = 2\,\Omega$. The impedance-matching *LC* circuit is shown in **Figure 16**. The desired shunt capacitor $C_{shunt}$ = 0.42 nF is obtained from Eq. (4) and Eq. (5). From Eq. (6), the total circuit factor $Q_T$ is 25.1

$$L_A = \frac{jX_A}{j\omega} \tag{4}$$

$$C_{shunt} = \frac{1}{L_A\omega^2} \tag{5}$$

$$Q_T = \frac{1}{R_A}\sqrt{\frac{L_A}{C_{shunt}+C_{chip}}} \tag{6}$$

The response of impedance-matching *LC* circuit, shown in **Figure 17**, is designed at 25 MHz with 3-dB bandwidth of 35 MHz. This impedance-matching *LC* circuit can be used with the RFID tag.

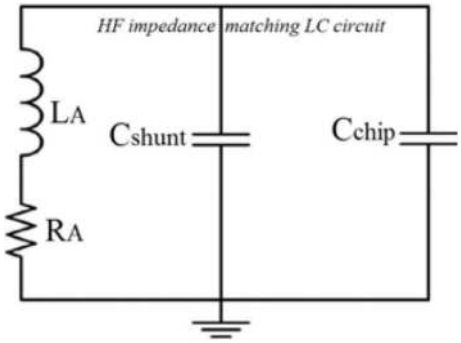


**Figure 16.** HF impedance-matching *LC* circuit.

To summarize in Section 3, the design of a novel single-radiator card-type tag antenna was presented. The tag antenna was implemented using series Hilbert-curve loop and matched stub. The design merges together the series Hilbert-curve HF coil with a square-loop UHF antenna to realize a singular radiator for an RFID tag that satisfies the commercial requirements of compact design and dual-band functionality. The tag exhibits good broadband and circular polarization response, and has a small physical footprint which can be easily manufactured. The antenna operates over the UHF band (400 MHz to 1 GHz) with a return loss better than -10 dB. The matching network was designed and integrated with the RFID chip with knowledge of the inductive impedance of the tag at various frequencies. The RFID tag predominately radiates quasi omnidirectionally in both the orthogonal *xy*- and *yz*-planes. The properties of the antenna make it suitable for various applications at HF and UHF bands.

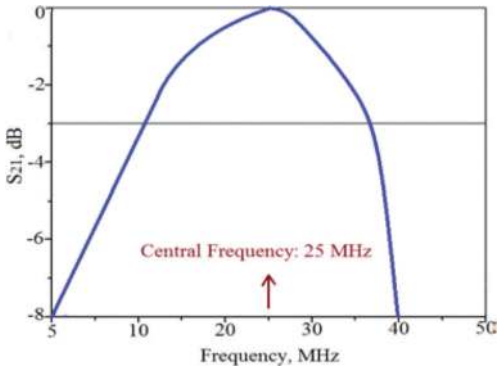


**Figure 17.** Impedance-matching *LC* circuit response.

## Acknowledgements

The authors would like to give special thanks to faculty of Microelectronics for financial support.

## Author details

Mohammad Alibakhshi-Kenari[1,*], Mohammad Naser Moghadasi[2], Ramazan Ali Sadeghzadeh[3], Bal Singh Virdee[4] and Ernesto Limiti[1]

*Address all correspondence to: naeem.alibakhshi@yahoo.com

1 Department of Electronic Engineering, University of Rome Tor Vergata, Rome, Italy

2 Faculty of Engineering, Science and Research Branch, Islamic Azad University, Tehran, Iran

3 Faculty of Electrical Engineering, K. N. Toosi University of Technology, Tehran, Iran

4 London Metropolitan University, Center for Communications Technology, London, UK

## References

[1] S. Lim, C. Caloz, T. Itoh, "Metamaterial-Based Electronically Controlled Transmission-Line Structure as a Novel Leaky-Wave Antenna with Tunable Radiation Angle and Beamwidth," *IEEE Transactions on Microwave Theory and Techniques*, 2005; 53(1): 161–173. DOI: 10.1109/TMTT.2004.839927

[2] C. Caloz, T. Itoh, "Array Factor Approach of Leaky-Wave Antennas and Application to 1-D/2-D Composite Right/Left-Handed (CRLH) Structures," *IEEE Microwave and Wireless Components Letters,* 2004; 14(6): 274–276. DOI: 10.1109/LMWC.2004.828009

[3] A. Neto, S. Bruni, G. Gerini, M. Sabbadini, "The Leaky Lens: A Broad-Band Fixed-Beam Leaky-Wave Antenna," *IEEE Transactions on Antennas Propagation*, 2005; 53(10): 3240–3246. DOI: 10.1109/TAP.2005.856351

[4] A. Toccafondi, C.D. Giovampaola, F. Mariottini, A. Cucini, "UHF-HF RFID Integrated Tag for Moving Vehicle Identification," *IEEE Antennas Propagation International Symposium Digest*, 2009: 1–4. DOI: 10.1109/APS.2009.5171707

[5] L.W. Mayer, A.L. Scholtz, "A Dual-Band HF/UHF Antenna for RFID Tags," *Proceedings of IEEE 68th Vehicular Technology Conference*,2008: 1–5.

[6] P. Iliev, P.L. Thuc, C. Luxey, R. Staraj, "Dual-Band HF-UHF RFID Tag Antenna," *Electronics Letters*,2009; 45: 439–441.

[7] R.H. Zeng, Q.X. Chu, "A Compact Slot-Coupled Dual-Band RFID Tag Antenna," *Microwave and Optical Technology Letters*,2009; 51(9): 2046–2048.

[8] Y.C. Lee, J.S. Sun, "A Fractal Dipole Tag Antenna for RFID Dual-Band Application," *Microwave and Optical Technology Letters*,2008; 50(7); 1963–1966.

[9] A. Attaran, R. Rashidzadeh, R. Muscedere, "Chipless RFIDTag Using RF MEMS Switch,"*Electronics Letters*,2014; 50(23): 1720–1722. DOI: 10.1049/EL.2014.3075

[10] Y.B. Ouattara, C. Hamouda, B. Poussot, J.M. Laheurte, "Compact Diversity Antenna for UHF RFIDReaders," *Electronics Letters*, 2012; 48(16): 975–977. DOI: 10.1049/EL.2012.1805

[11] K.S. Leong, M.L. Ng, P.H. Cole, "Miniaturization of Dual Frequency RFID Antenna with High Frequency Ratio," *IEEE Antennas Propagation International Symposium Digest*, 2011: 5475–5478.

[12] J.S. Kuo, J.J. Wang, C.Y. Huang, "Dual-Frequency Antenna for RFID Tags with Complementary Characteristic," *Microwave and Optical Technology Letters*, 2007; 49(6): 1396–1398.

[13] F. Paredes, G.Z. Gonzàlez, J. Bonache, F. Martín, "Dual-Band Impedance-Matching Networks Based on Split-Ring Resonators for Applications in RF Identification (RFID)," *IEEE Transactions on Microwave Theory and Techniques*, 2010; 58(5): 1159–1166.

[14] Y. Nishioka, K. Hitomi, H. Okegawa, T. Mizuno, T. Fukasawa, H. Miyashita, Y. Konishi, "Novel Antenna Configuration for HF and UHF Band Hybrid Card-Type RFID Tags," *Antennas and Propagation (EuCAP)*, 2010: 1–5.

[15] Z.L. Ma, L.J. Jiang, J. Xi, T.T. Ye, "A Single-Layer Compact HF-UHF Dual-Band RFID Tag Antenna," *IEEE Antennas Wireless Propagation Letters*, 2012; 11: 1257–1260.

[16] T. Deleruyelle, P. Pannier, M. Egels, E. Bergeret, "Dual Band Mono-Chip HF-UHF Tag Antenna," *Antennas and Propagation Society International Symposium (APSURSI)*, 2010: 1–4.

[17] Y. Pan, L. Zheng, H.J. Liu, J.Y. Wang, R.L. Li, "Directly-Fed Single-Layer Wideband RFIDReader Antenna," *Electronics Letters*, 2012; 48(11): 607–608.

[18] G.H. Du, T. Tang, Y. Deng, "Dual-band metal skin UHF RFID tag antenna", *Electronics Letters*, 2013; 49(14): 858–860.

[19] J. Anguera, C. Puente, E. Martínez, E. Rozan, "The Fractal Hilbert Monopole: A Two-Dimensional Wire," *Microwave and Optical Technology Letters*, 2003; 36(2): 102–104.

[20] J. Zhu, A. Hoorfar, N. Engheta, "Feed-Point effects in Hilbert-Curve Antennas," *IEEE Antennas and Propagation Society International Symposium, URSI Digest*, 2002: 6623–6626.

[21] J. Anguera, C. Puente, C. Borja, J. Soler, "Fractal-Shaped Antennas: a Review," *Wiley Encyclopedia of RF and Microwave Engineering*, 2005; 2: 1620–1635.

[22] D. Gala, J. Soler, C. Puente, C. Borja, J. Anguera, "Miniature Microstrip Patch Antenna Loaded with a Space-Filling Line Based on the Fractal Hilbert Curve," *Microwave and Optical Technology Letters*, 2003; 38(4): 311–312.

[23] I. Sanz, J. Anguera, A. Andú,jar, C. Puente, C. Borja, "The Hilbert Monopole Revisited," *European Conference on Antennas and Propagation, EuCAP*, 2010.

[24] K.J. Vinoy, K.A. Jose, V.K. Varadan, V.V. Varadan, "Hilbert Curve Fractal Antenna: A Small Resonant Antenna for VHF/UHF applications," *Microwave and Optical Technology Letters*, 2001; 29(4): 215–1219.

[25] K.J. Vinoy, K.A. Jose, V.K. Varadan, V.V. Varadan, "Resonant Frequency of Hilbert Curve Fractal Antenna," *IEEE APS*, 2001; 3: 648–651.

[26] M.Z. Azad, M. Ali, "A Miniaturized Hilbert PIFA for Dual-Band Mobile Wireless Applications," *IEEE Antennas and Wireless Propagation Letters*, 2005; 4: 59–62.

[27] J.C. Liu, B.H. Zeng, I. Chen, C.C. Chang, D.C. Chang, "An Inductive Self-Complementary Hilbert-Curve Antenna for UHF RFID Broadband and Circular-Polarization Tags," *Progress in Electromagnetic Research B*, 2009; 16: 433–443.

[28] Ansoft HFSS, www.ansoft.com/products/hf/hfss.

[29] Y. Nishioka, K. Hitomi, H. Okegawa, T. Mizuno, T. Fukasawa, H. Miyashita, Y. Konishi, "Novel Antenna Configuration for HF and UHF Band Hybrid Card-Type RFID Tags," *Antennas and Propagation (EuCAP)*, 2010: 1–5.

[30] Z.L. Ma, L.J. Jiang, J. Xi, T.T. Ye, "A Single-Layer Compact HF-UHF Dual-Band RFID Tag Antenna," *IEEE Antennas Wireless Propagation Letters*,2012; 11: 1257–1260. DOI: 10.1109/LAWP.2012.2225821

[31] S. Basat, S. Bhattacharya, A. Rida, S. Johnston, L. Yang, M.M. Tentzeris, J. Laskar, "Fabrication and Assembly of a Novel High-Efficiency UHF RFID Tag on Flexible LCP substrate," *IEEE Electronic Components and Technology Conference*, 2006: 1352–1355.

[32] Specifications, ISO15693, ISO18000-3, Elastic RFID Tech Co.